# CMS Physics Analysis Summary

Contact: cms-phys-conveners-ftr@cern.ch 2018/12/11

# Vector Boson Scattering prospective studies in the ZZ fully leptonic decay channel for the High-Luminosity and High-Energy LHC upgrades

The CMS Collaboration

## Abstract

Prospective studies for the vector boson scattering (VBS) in the ZZ channel at the HL-LHC are presented, where the Z bosons are identified and measured through their leptonic decays, $\ell = e, \mu$. The results obtained from the 2016 analysis with an integrated luminosity of 36 fb$^{-1}$ are projected to the HL-LHC luminosity of 3000 fb$^{-1}$ and center-of-mass energy of 14 TeV, taking into account the increased acceptance of the CMS detector. The projected uncertainty in the VBS ZZ cross section is 8.5–10.3% depending on the lepton $\eta$ coverage and assumptions made for the systematic uncertainties. A study is performed to separate the longitudinal polarization ($Z_L$) from the dominant transverse polarizations. The expected sensitivity for the VBS $Z_L Z_L$ fraction is 1.4 standard deviations. The foreseen upgrade coverage of up to $|\eta| = 3(2.8)$ for electrons (muons) leads to a 13% improvement in sensitivity compared to the Run 2 acceptance. Extending the coverage for electrons up to $|\eta| = 4$ would result in a modest increase in the sensitivity. Finally, the HE-LHC option would allow to bring the sensitivity at the $5\sigma$ level for this process.

# 1 Introduction

The high-luminosity LHC (HL-LHC) will operate at the center-of-mass (c.o.m) energy of 14 TeV and is expected to deliver to each experiment integrated luminosities of up to 3000 $fb^{-1}$. It will provide a unique opportunity to search for rare physics processes. Weak vector boson scattering (VBS) is intimately related to the electroweak (EW) symmetry breaking mechanism (EWSB), the longitudinal mode of the gauge bosons being identified in the standard model (SM) with the Goldstone bosons of the EWSB. Unitarity restoration in the scattering of longitudinal weak bosons relies on the interference of the scattering amplitudes involving gauge couplings and couplings to the Higgs boson. While the studies of VBS have already been performed at the LHC Run 2 [1–4], the HL-LHC is expected to provide the first opportunity to study the longitudinal scattering of weak bosons.

Figure 1 shows some of the Feynman diagrams that contribute to EW production of the ZZjj signature, involving quartic (top left) and trilinear vertices (top right), as well as diagrams involving the Higgs boson (bottom left). The $qq \to ZZjj$ process can also be mediated through the strong interaction (bottom right in Fig. 1), which leads to the same final state as the VBS signal, and therefore constitutes an irreducible background.

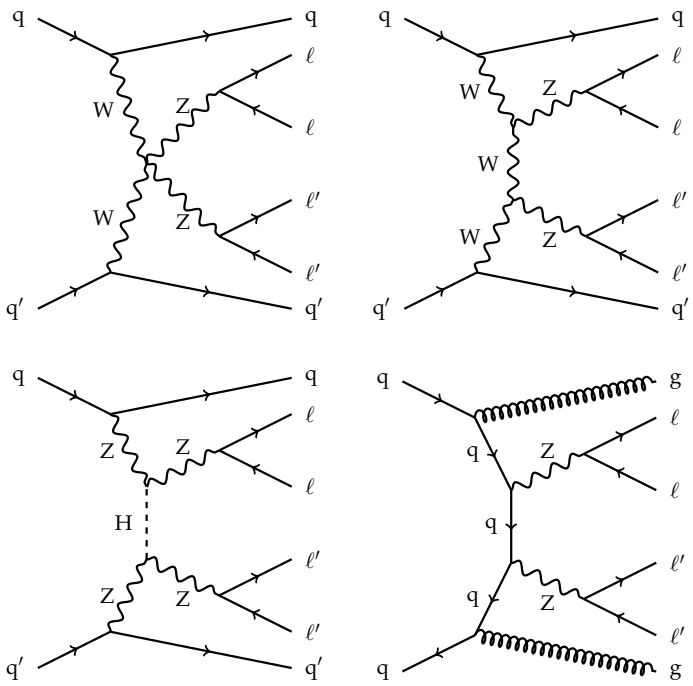


Figure 1: Representative Feynman diagrams for the EW- (top row and bottom left) and QCD-induced production (bottom right) of the ZZjj $\to \ell\ell\ell'\ell'$jj ($\ell$, $\ell' =$ e or $\mu$) final state. The scattering of massive gauge bosons as depicted in the top row is unitarized by the interference with amplitudes that feature the Higgs boson (bottom left).

This note presents prospective studies performed for VBS in the ZZ fully leptonic decay channel at the HL-LHC. It is based on the experimental investigation of VBS in the ZZ channel performed using data corresponding to an integrated luminosity of 36 $fb^{-1}$ collected in 2016 and exploiting the fully leptonic final state, where both Z bosons decay into electrons or muons, $ZZ \to \ell\ell\ell'\ell'$ ($\ell$, $\ell' =$ e or $\mu$) [1]. Despite a low cross section, a small $Z \to \ell\ell$ branching fraction, and a large irreducible QCD background, this channel provides a favorable laboratory to

study EWSB since all final-state particles are precisely reconstructed. In addition to a negligible reducible background, this channel provides a precise knowledge of the scattering energy through the measurement of $m_{4l}$. Furthermore, the measurement of the spin correlations of the final state fermions enables to identify the longitudinal contribution, which is the main interest of such studies. The longitudinal Z bosons ($Z_L$) are expected to be dominantly produced in the forward region [5], therefore a particular attention is payed on the lepton pseudorapidity coverage in the presented study.

The projected sensitivity for VBS ZZ is estimated by scaling the expected yields for the signal and the background processes, taking into account the increase in luminosity and scattering energy as well as the changes in acceptance and selection efficiencies between the Run 2 (13 TeV) and the Phase-2 (14 TeV) configurations. The Delphes simulation [6] is then used to assess the sensitivity to VBS $Z_L Z_L$.

After a brief reminder of the CMS detector Phase-2 upgrade in Section 2, the simulated samples used in this analysis are described in Section 3. The event selection and analysis strategy are then presented in Section 4. The effect of the increased acceptance and center-of-mass energy are discussed in Section 5 and the systematic uncertainties are addressed in Section 6. The sensitivity results for the VBS ZZ measurement at HL-LHC are presented in Section 7. The separation of the longitudinal component and results for the expected sensitivity and precision for the VBS $Z_L Z_L$ measurement are presented in Section 9. A summary of the analysis and results is given in Section 10.

## 2 CMS detector upgrade

The upgraded CERN High-Luminosity LHC is expected to deliver a peak instantaneous luminosity of up to $7.5 \times 10^{34}\,\mathrm{cm^{-2}\,s^{-1}}$ [7], which is an increase in instantaneous luminosity of about four times with respect to the LHC Run 2 performance. With this increase in instantaneous luminosity, the number of overlapping proton-proton interactions per bunch crossing, or pileup (PU), is expected to increase from its mean value of about 40 at the LHC to a mean value of up to 200 at the HL-LHC. Similarly, the levels of radiation are expected to significantly increase in all regions of the detector, in particular in its forward regions.

The CMS detector [8] will be substantially upgraded in order to fully exploit the physics potential offered by the increase in luminosity, and to cope with the demanding operational conditions at the HL-LHC [9–13]. In particular, in order to sustain the increased PU rate and associated increase in flux of particles, the upgrade will provide the detector with: higher granularity to reduce the average channel occupancy, increased bandwidth to accommodate the higher data rates, and improved trigger capability to keep the trigger rate at an acceptable level without compromising physics potential. The upgrade will also provide an improved radiation hardness to withstand the increased radiation levels.

The upgrade of the first level hardware trigger (L1) will allow for an increase of L1 rate and latency to about 750 kHz and 12.5 $\mu$s, respectively. The upgraded L1 will also feature inputs from the silicon strip tracker, allowing for real-time track fitting and particle-flow reconstruction [14] of objects at the trigger level. The high-level software trigger (HLT) is expected to reduce the rate by about a factor of 100 to 7.5 kHz.

The entire pixel and strip tracker detectors will be replaced to increase the granularity, reduce the material budget in the tracking volume, improve the radiation hardness, and extend the geometrical coverage and provide efficient tracking up to pseudorapidities of about $|\eta| = 4$.

In addition, the tracker will provide information on tracks above a configurable transverse momentum threshold to the L1 trigger, information presently only available at the HLT. It will also allow for including tracks with low momentum ( $\approx 2\,\text{GeV}$).

The muon system will be enhanced by upgrading the electronics of the cathode strip chambers (CSC), resistive plate chambers (RPC) and drift tubes (DT). New muon detectors based on improved RPC and gas electron multiplier (GEM) technologies will be installed to add redundancy, increase the geometrical coverage up to about $|\eta| = 2.8$, and improve the trigger and reconstruction performance in the forward region.

The barrel electromagnetic calorimeter (ECAL) will be operated at lower temperatures to mitigate noise in avalanche photodiodes (APDs) due to radiation damage. Its upgraded front-end electronics will be able to exploit the information from single crystals at the L1 trigger level, to accommodate trigger latency and bandwidth requirements, and to provide an increased sampling rate of 160 MHz and high-precision timing capabilities. The hadronic calorimeter (HCAL), consisting in the barrel region of brass absorber plates and plastic scintillator layers, will be read out by silicon photomultipliers (SiPMs).

The endcap electromagnetic and hadron calorimeters will be replaced with a new combined sampling calorimeter (HGCal) that will provide coverage in pseudorapidity from about $|\eta| = 1.5$ up to $|\eta| = 3$. The new calorimeter will be based on a lead tungsten followed by stainless steel absorber with silicon sensors as the active material in the front section, and it will feature plastic scintillator tiles readout by SiPMs towards its back section at large distances from the beam. It will provide highly-segmented spatial information in both transverse and longitudinal directions, as well as 160 MHz sampling allowing high-precision timing capability for photons, which will allow for improved PU rejection and identification of electrons, photons, tau leptons, and jets.

Finally, the addition of a new precision timing detector for minimum ionizing particles (MTD) in both the barrel and endcap regions is envisaged to provide the capability for 4-dimensional reconstruction of interaction vertices that will significantly offset the CMS performance degradation due to high PU rates. The MTD is expected to achieve timing resolution of about 30 to 40 ps, and will provide coverage up to pseudorapidities of about $|\eta| = 3$.

A detailed overview of the CMS detector upgrade program is presented in Ref. [9–13]. The expected performance of the reconstruction algorithms and PU mitigation with the CMS detector is summarized in Ref. [15].

# 3 Monte Carlo samples and simulation

In addition to the samples used for the 13 TeV 2016 analysis and described in Ref. [1], simulated signal samples were produced for center-of-mass energies of $\sqrt{s} = 14$ and 13 TeV with polarization information on the outgoing Z bosons. Samples of simulated events for the main QCD background process were also produced for the center-of-mass energy of $\sqrt{s} = 14$ TeV.

The signal samples from purely electroweak VBS production, referred to as EW ZZ, are generated using MADGRAPH version 5.4.2 [16] and leading order (LO) version of PDFset NNPDF3.0 [17] with $\alpha_s = 0.13$ and using the 4-flavour scheme. The polarization information of individual Z bosons is kept by using the DECAY package from MADGRAPH5_aMC@NLO version 1.5.14 instead of MADSPIN. The 14 TeV sample is used to study the kinematics of polarized EW ZZ production and optimize the separation of the longitudinal component. The signal sample at 13 TeV is used to assess the effect of the change in center-of-mass energy.

Samples of events for the main irreducible QCD-induced pp $\rightarrow$ ZZjj process, referred to as QCD qqZZ, are produced at 14 TeV at next-to-leading-order (NLO) with up to two extra parton emissions with `MadGraph5_aMCatNLO` [18], and merged with parton showers using the FxFx scheme [19]. The jet multiplicities are simulated separately, in a similar way as was done in Ref. [1]. These samples are used to assess the effect of the change of center-of mass energy.

The PYTHIA v8.2 [20, 21] package is used for parton showering, hadronization and underlying event simulation. The fast-simulation package Delphes [6], with the CMS detector configuration corresponding to a number of pileup interactions of 200 (refered to as the 200PU configuration), is then used to simulate the expected response of the upgraded CMS detector.

## 4 Event selection and analysis

The analysis is based on the Run 2 investigation of VBS in the ZZ channel described in Ref. [1], with a data set corresponding to an integrated luminosity of 36 fb$^{-1}$. Run 2 results are projected into HL-LHC conditions, taking into account the effects of the increased lepton acceptance and center-of-mass energy in addition to the expected integrated luminosity.

The final state should contain at least two pairs of oppositely charged isolated leptons and at least two hadronic jets. The ZZ selection used is similar to that used in the CMS inclusive ZZ cross section measurement [22]. Events are required to contain at least two Z candidates, each formed from pairs of isolated and identified electrons or muons of opposite charges. Only reconstructed electrons (muons) with a $p_{\mathrm{T}} > 7\,(5)$ GeV are considered. Among the four leptons, the highest $p_{\mathrm{T}}$ lepton must have $p_{\mathrm{T}} > 20\,\mathrm{GeV}$, and the second-highest $p_{\mathrm{T}}$ lepton must have $p_{\mathrm{T}} > 12\ (10)\,\mathrm{GeV}$ if it is an electron (muon). Each pair of oppositely charged same-flavor leptons, is required to satisfy $60 < m_{\ell\ell} < 120\,\mathrm{GeV}$. At least two jets with $p_{\mathrm{T}} > 30\,\mathrm{GeV}$ and $|\eta| < 4.7$ are additionaly required. The two highest $p_{\mathrm{T}}$ jets are referred to as the tagging jets and their invariant mass is required to be larger than 100 GeV. The above loose requirements defined the ZZjj selection used to extract the VBS signal.

The dominant background to the VBS search is the QCD-induced production of two Z bosons in association with jets. The yield and shape of the multivariate discriminant of this irreducible background is taken from simulation, but ultimately constrained by the data in the fit that extracts the EW signal. Reducible backgrounds arise from processes in which heavy-flavor jets produce secondary leptons or from processes in which jets are misidentified as leptons. The lepton identification and isolation and invariant mass requirements strongly suppress these backgrounds, which, after the selection, have a negligible impact on the results.

The determination of the signal strength for the EW production (ratio of the measured cross section to the SM expectation) employs a multivariate discriminant based on a boosted decision tree (BDT) to optimally separate the signal and the QCD background. Seven observables are used in the BDT, including $m_{\mathrm{jj}}$, $|\Delta\eta_{\mathrm{jj}}|$, $m_{\mathrm{ZZ}}$, as well as the Zeppenfeld variables [23] $\eta^{*}_{\mathrm{Z}_i} = \eta_{\mathrm{Z}_i} - (\eta_{\mathrm{jet\,1}} + \eta_{\mathrm{jet\,2}})/2$ of the two Z bosons, and the ratio between the $p_{\mathrm{T}}$ of the tagging jet system and the scalar $p_{\mathrm{T}}$ sum of the tagging jets ($R(p_{\mathrm{T}})^{\mathrm{jets}}$). The BDT also exploits the event balance $R(p_{\mathrm{T}})^{\mathrm{hard}}$, which is defined as the transverse component of the vector sum of the Z bosons and tagging jets momenta, normalized to the scalar $p_{\mathrm{T}}$ sum of the same objects [24]. The tunable hyper-parameters of the BDT training algorithm are optimized via a grid-search algorithm and the BDT performance was checked using a matrix element approach [25–27].

A maximum likelihood fit of the BDT distributions for signal and backgrounds is used to extract the signal strength. The shape and normalization of each distribution are allowed to vary

within their respective uncertainties. The systematic uncertainties are treated as nuisance parameters in the fit and profiled.

# 5 Effect of the increased energy and acceptance

In addition to the luminosity scaling, a first effect comes from the difference in center-of-mass energy for the Run 2 (13 TeV) and the HL-LHC (14 TeV) configurations.

The cross sections are evaluated at LO with MADGRAPH (v5.4.2) [16] for the EW signal and the QCD qqZZ background, and with MCFM [28] for the QCD ggZZ background. The cross section ratio for the different processes are reported in Table 1. The signal cross section increases by about 15% while for the QCD qqZZ (ggZZ) background the increase is of about 17% (13%). The cross section ratios for the HE-LHC configuration (27 TeV) with respect to the HL-LHC configuration (14 TeV) is also reported.

Table 1: Cross section ratios $\sigma_{14\,\text{TeV}}$ / $\sigma_{13\,\text{TeV}}$ and $\sigma_{27\,\text{TeV}}$ / $\sigma_{14\,\text{TeV}}$ for the EW signal and the QCD background processes.

| | EW ZZ | QCD qqZZ | QCD ggZZ |
|---|---|---|---|
| $\sigma_{14\,\text{TeV}}$ / $\sigma_{13\,\text{TeV}}$ | 1.15 | 1.17 | 1.13 |
| $\sigma_{27\,\text{TeV}}$ / $\sigma_{14\,\text{TeV}}$ | 3.25 | 3.41 | 3.57 |

A second order effect arises from the difference in event acceptance between the two energies. It is estimated for each process at the reconstructed level with the 200PU configuration. The corrections are found to be small, up to $\sim 6\%$. It has been checked for all the observables used as input to the BDT that the shape differences induced by the change in center-of-mass energy are small.

The ratio of acceptances for various $\eta$ coverage configurations and for a center-of-mass energy of 13 TeV are reported in Table 2.

Table 2: Acceptance ratios for the Phase-2 detector with respect to Run 2 for various $\eta$ coverage configurations. The first number denotes the cut value for electrons while the number in parentheses denotes the cut value for muons. The numbers are for the center-of-mass energy of 13 TeV.

| | EW ZZ | QCD qqZZ | QCD ggZZ |
|---|---|---|---|
| $\lvert\eta\rvert < 3.0(2.8)/\lvert\eta\rvert < 2.5(2.4)$ | 1.13 | 1.18 | 1.12 |
| $\lvert\eta\rvert < 4.0(2.8)/\lvert\eta\rvert < 2.5(2.4)$ | 1.21 | 1.33 | 1.15 |

The increase in signal yield from the increased lepton acceptance for the Phase-2 detector is up to $\sim 20\%$. One can see also that an extension of up to $|\eta| < 4$ provides a sizeable increase in signal event yield, compared to $|\eta| < 3$. The event yield increase for the QCD qqZZ background is $\sim 10\%$ higher than for the signal. The increase for the loop-induced ggZZ background is significantly lower, due to the Z production being more central for this process.

The shape differences induced on the variables used in the BDT by the change in detector acceptance at a given energy are found to be small. The most important difference appears for

the Zeppenfeld variables as can be expected since these variables directly relate to the pseudo-rapidity of the final state Z bosons and therefore on the decay leptons. The change in $m_{jj}$ and $\Delta\eta_{jj}$, which weigh the most in the BDT discriminant, is very small.

## 6 Systematic uncertainties

In order to project the expected significance to HL-LHC configuration, two scenarios are considered for the systematic uncertainties. The first scenario ('Run 2 scenario') consists in using the same systematic uncertainties as that used for the Run 2 analysis, apart from the uncertainty in the QCD ggZZ background yield. In the second scenario ('YR18 scenario'), improved systematic uncertainties are assumed to be obtained from the more data and better understanding of the detector. In this scenario, the theory systematic uncertainties (PDF and QCD scales) are furthermore halved with respect to the Run 2 scenario.

Both shape and yield variations of the BDT output distributions for the signal and the various background are considered, in the same way as done for the Run 2 analysis [1].

For all processes apart from the sub-leading QCD ggZZ background, theoretical uncertainties were estimated by simultaneously varying the renormalization and factorization scales up and down by a factor of two with respect to the nominal value. As a VBS process the signal exhibits a weak dependence on the QCD scales choice and the size of the observed effect was found compatible with the NLO-LO comparison carried out in Ref. [29]. Uncertainties related to the choice of the PDF and strong coupling constant were evaluated following the PDF4LHC [30, 31] prescription and using the NNPDF [32] PDF sets. This procedure is also applied to the minor ttZ and WWZ backgrounds which have a negligible impact on the signal sensitivity.

The uncertainty associated to the QCD ggZZ background deserved a particular treatment. The $gg \to ZZjj$ loop-induced background, despite being suppressed by two order in $\alpha_S$ compared to the leading $qq \to ZZjj$, contributes significantly in the signal region. The kinematical distributions and in particular $m_{jj}$ appeared to be more signal-like. Being an $\alpha_S^4$ process at LO, this process is difficult to model and a flat uncertainty of 40% was assigned from the comparison of an MCFM simulation of $gg \to ZZ$ [28], therefore with the two extra jets from parton showers, and a MADGRAPH simulation of the QCD ggZZ background $gg \to ZZjj$.

The large uncertainty in the ggZZ loop-induced background yield has the highest impact on the significance, and is among the dominant uncertainties for the cross section measurement. Therefore, in addition to the values quoted in Table 3 for the YR18 scenario, the precision on the cross section measurement is also presented as a function of the uncertainty in the QCD ggZZ loop-induced background yield.

The experimental uncertainties are taken from the Run 2 analysis [1]. They include an uncertainty in the trigger efficiency, an uncertainty in the lepton selection efficiency (the numbers given in Table 3 stands for the $4e/2e2\mu/4\mu$ final states, respectively) and an uncertainty in the pileup modeling estimated by varying the minimum bias cross section in the simulation by $\pm 4.6\%$. The jet energy scale (JES) uncertainty was estimated by varying the $p_T$ of the tagging jets by their respective uncertainty. The jet energy resolution (JER) in the simulation was corrected to match the distribution observed in the data and the uncertainty in the JER scaling factor is propagated to the simulated jets. The uncertainty in the data-driven reducible background, dominated by the statistic available in the control region, is sizeable but had a negligible effect on the sensitivity. The uncertainty in the luminosity is included as well.

The main source of systematic uncertainties and their effect on the signal and background

yields are listed in Table 3. Other uncertainties in the minor ttZ and WWZ backgrounds are considered as well but are not listed in Table 3 as they have a negligible impact on the sensitivity.

Table 3: Effect of the systematic uncertainties on the signal and backgrounds yields for the two considered scenarios.

| Systematic source | Run 2 scenario | YR18 scenario |
|---|---|---|
| QCD scale, EW ZZ signal | 1–10% (shape) | 5% |
| PDF, EW ZZ signal | 8% (shape) | 4% |
| QCD scale, QCD qqZZ background | 8–12% (shape) | 6% |
| PDF, QCD qqZZ background | 3% (shape) | 1.5% |
| QCD ggZZ background | 10% | 10% or varied |
| Luminosity | 2.6% | 1% |
| Trigger efficiency | 2% | 1% |
| Lepton reco and selection efficiency | 6/4/2% | 2/1/0.5% |
| JES, EW ZZ signal | 1–5% (shape) | 1% |
| JER, EW ZZ signal | 1–2% (shape) | 1% |
| JES, QCD qqZZ background | 10–20% (shape) | 10% |
| JER, QCD qqZZ background | 3–6% (shape) | 1% |

For the cross section measurement, it is assumed that a fiducial cross section will be measured in a fiducial volume close to the detector level, such that the measurement is to first order insensitive to the theoretical uncertainties in the EW ZZ signal. Therefore, for this measurement, the nuisances corresponding to the EW ZZ signal uncertainties are frozen in the fit.

# 7 Results for VBS ZZ

The projected signal and background yields for the ZZjj selection defined in Section 5 and used in the statistical analysis, as well as for a VBS-enriched cut-based selection also requiring $m_{jj} > 400\,\text{GeV}$ and $|\Delta\eta_{jj}| > 2.4$, are reported in Table 4. The yields are given for an integrated luminosity of 3000 $\text{fb}^{-1}$. The reported uncertainties correspond to the Run 2 scenario, together with an uncertainty of 40% on the QCD ggZZ background yield as used for the Run 2 analysis. The reported event yields include the correction factors to account for the extended acceptance and the increase in center-of-mass energy as presented in Section 5. For the minor Z+X, ttZ and WWZ backgrounds, a correction factor similar to that evaluated for qqZZ is used. The corrections for the yields of these minor backgrounds lead to a change in projected significance of less than 1%.

A total of $\sim 705$ events are expected for the VBS ZZ process in the fully leptonic final states for an integrated luminosity of 3000 $\text{fb}^{-1}$.

Figure 2 shows the scaled BDT output distribution for the signal and the various backgrounds for an integrated luminosity of 3000 $\text{fb}^{-1}$. The points represent pseudodata generated from the sum of the expected contributions of each process.

Figure 3 shows the projected significance for a 10% uncertainty in QCD ggZZ background yield, as a function of the integrated luminosity and for the two scenarios described in Section 6, as well as for a scenario with only the statistical uncertainty included. A sensitivity of $5\sigma$, where $\sigma$ stands for the standard deviation, is reached for an integrated luminosity of 225 $\text{fb}^{-1}$

Table 4: Signal and background yields projections for the ZZjj inclusive selection used in the statistical analysis and for a VBS cut-based selection also requiring $m_{jj} > 400\,\text{GeV}$ and $|\Delta\eta_{jj}| > 2.4$. Quoted uncertainties correspond to the systematic uncertainties for the Run 2 scenario together with a 40% uncertainty in the QCD ggZZ background yield, as used for the Run 2 analysis.

| Selection | $t\bar{t}Z$ and WWZ | QCD qqZZ + ggZZ | Total bkg. | EW ZZ signal | Total expected |
|---|---|---|---|---|---|
| ZZjj | $876 \pm 99$ | $11900 \pm 1700$ | $13600 \pm 1700$ | $706 \pm 79$ | $14300 \pm 1700$ |
| VBS cuts | $111 \pm 25$ | $2340 \pm 490$ | $2530 \pm 510$ | $456 \pm 57$ | $2990 \pm 480$ |

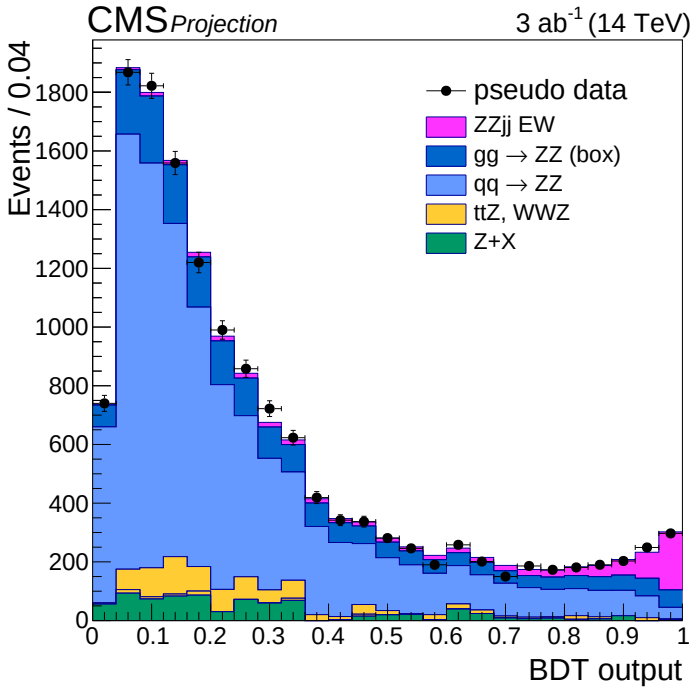


Figure 2: Expected distribution of the BDT output for 3000 $\text{fb}^{-1}$. The points represent pseudo data generated from the sum of the expected contributions for each process. The purple filled histogram represents the EW signal, the dark blue the QCD ggZZ background, the light blue the QCD qqZZ background, the yellow the ttZ plus WWZ backgrounds and the green the reducible background.

if considering the statistical uncertainties only. It is reached for 280 (260) $\text{fb}^{-1}$ if considering the systematic uncertainties of the Run 2 (YR18) scenario.

The expected significance for the Run 2 (YR18) scenario and for a 10% uncertainty in the QCD ggZZ background yield is 13.0 (13.6) for an integrated luminosity of 3000 $\text{fb}^{-1}$.

Figure 4 shows the projected relative uncertainty in the cross section measurement for 3000 $\text{fb}^{-1}$ as a function of the dominant systematic uncertainty, considering the YR18 scenario for the other uncertainties. Improving the uncertainty in the QCD ggZZ background from 40% to 5% leads to an improvement on the projected uncertainty in the cross section measurement of $\sim 13\%$.

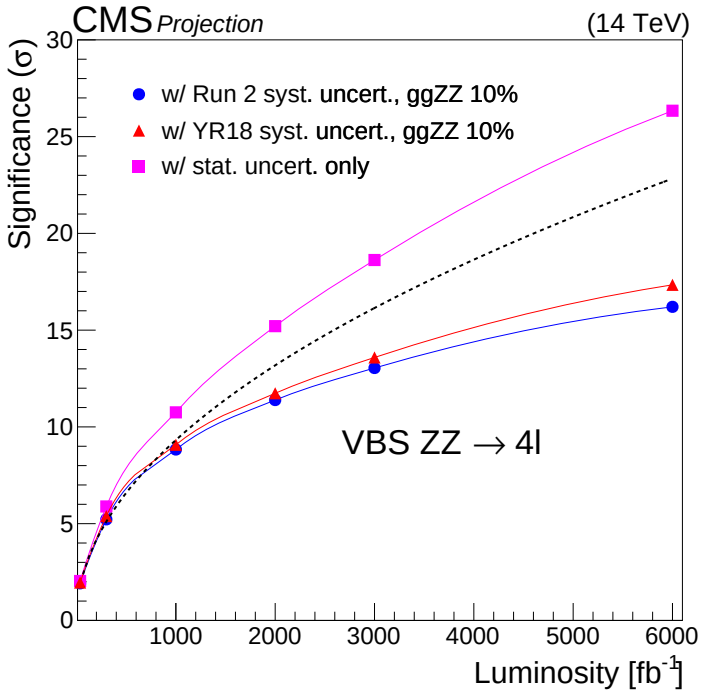


Figure 3: Projected significance for a 10% uncertainty in the QCD ggZZ background yield as a function of the integrated luminosity and for all other systematic uncertainties according to the Run 2 scenario (blue line and circles), and according to YR18 scenario (red line and triangles). The magenta line and squares show the results with only the statistical uncertainties included. The dashed line shows the projected significance as obtained scaling the 2016 result with statistical uncertainty only by the luminosity ratio.

Figure 5 shows the projected relative uncertainty in the cross section measurement as a function of the integrated luminosity and for the two scenarios described in Section 6, as well as for a scenario with only the statistical uncertainty included.

The projected measurement uncertainty is 9.5% (8.5%) for the Run 2 (YR18) scenario and for a 10% uncertainty in the QCD ggZZ background yield (blue filled circle and red filled triangle on Fig. 5), for an integrated luminosity of 3000 $\text{fb}^{-1}$. The projected measurement uncertainty is 10.3% (9.5%) for the Run 2 (YR18) scenario and for 3000 $\text{fb}^{-1}$ if considering only the luminosity increase. It is 9.8% (8.8%) if considering a pseudorapidity coverage of only up to $|\eta| = 3$ and 9.9% (9.0%) if considering a pseudorapidity coverage of only up to $|\eta| = 2.5$.

# 8 VBS $Z_L Z_L$ analysis

The decay angle $\cos\theta^*$ of the lepton direction in the Z decay rest frame with respect to the Z momentum direction in the laboratory frame is the most distinctive feature of the Z bosons polarisation states. The Z $p_T$ and $\eta$ distributions also carry information on the $Z_L Z_L$ production, in particular longitudinal Z bosons are produced with a lower $p_T$ and more forward, as compared to transverse polarizations ($Z_T$).

The distributions of $\cos\theta^*$, $p_T$ and $\eta$ of both Z bosons, together with the distributions of all observables previously used to separate the VBS process from the QCD backgrounds (see Section 4) are employed as input to a BDT to separate the VBS $Z_L Z_L$ signal from the VBS and QCD

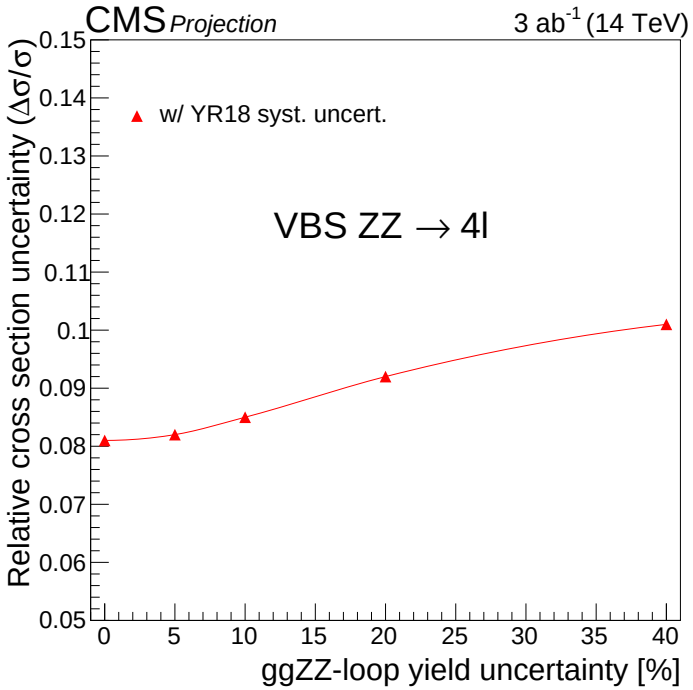


Figure 4: Projected relative uncertainty in the cross section for 3000 fb$^{-1}$ as a function of the uncertainty in the QCD ggZZ background yield (right). The YR18 scenario is used for the other systematic uncertainties.

backgrounds. Reducible backgrounds are expected to be very small and are therefore neglected in this study.

Figure 6 presents the distributions of some of the discriminant variables used, as obtained from Delphes simulation with 200PU configuration. $Z_1$ ($Z_2$) refers to the $p_T$-leading ($p_T$-subleading) Z boson. The inclusive ZZjj selection that requires $m_{jj} > 100$ GeV is applied. The distributions are normalized to unity for shape comparison.

The BDT is trained separately to discriminate the LL signal from the QCD backgrounds (QCD BDT) and to discriminate the LL signal from the VBS background (VBS BDT). For the training of the QCD BDT a single background is considered, constituted by a weighted mixture of the QCD qqZZ and QCD ggZZ backgrounds.

Cut values are defined on the QCD BDT and on the VBS BDT ouput values, which maximize the overall significance estimator $S/\sqrt{B}$ for the selected events. The corresponding signal efficiency is 14.1% and the VBS, QCD qqZZ and QCD ggZZ background efficiencies are 1.6%, 0.03% and 0.05%, respectively.

It is assumed that the VBS $Z_L Z_L$ fraction, defined as VBS $Z_L Z_L$/VBS $(Z_L Z_L + Z_L Z_T + Z_T Z_T)$ will be measured, rather than the absolute VBS $Z_L Z_L$ cross section. In such ratio measurement, the systematic uncertainties from luminosity, and selection efficiency, as well as theoretical uncertainties on the VBS and VBS background cross section cancel out, such that among the sources of systematic uncertainties listed in Table 3 only the uncertainties in the QCD qqZZ and ggZZ background yields are considered.

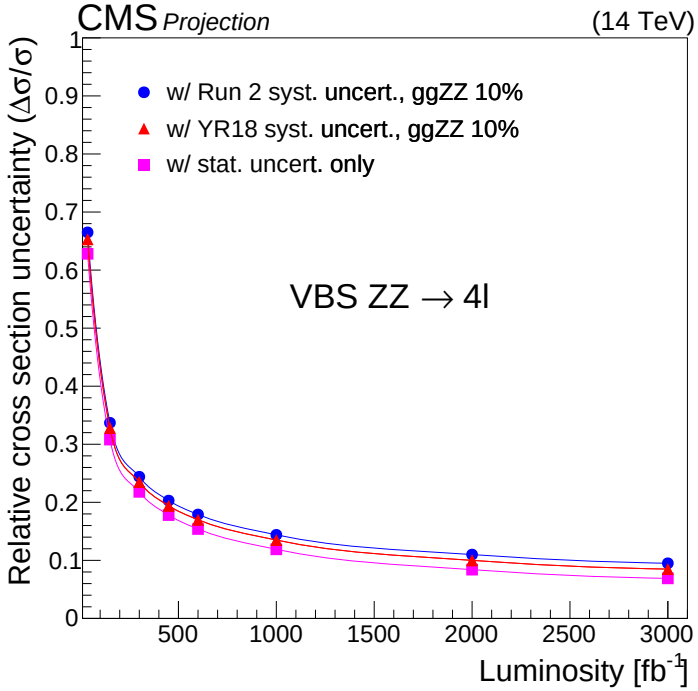


Figure 5: Projected relative uncertainty in the cross section as a function of the integrated luminosity and for all other systematic uncertainties according to the Run 2 scenario (blue line and circles), and according to the YR18 scenario (red line and triangles). Results are shown for 10% uncertainty uncertainty in the QCD ggZZ background yield. The magenta line and filled squares show the results with only the statistical uncertainties included.

## 9 Results for VBS $Z_L Z_L$

Figure 7 shows the expected significance for the VBS $Z_L Z_L$ fraction as a function of the integrated luminosity and for the scenarios described in Section 6 and for a 10% uncertainty in the ggZZ loop-induced background yield, as well as for a scenario with only the statistical uncertainty included. A significance of $1.4\sigma$ is reached for 3000 fb$^{-1}$. As expected from the ratio measurement, the effect of systematic uncertainties is very small. Results are also shown for an integrated luminosity of 6000 fb$^{-1}$, which would approximately correspond to combining ATLAS and CMS after 3000 fb$^{-1}$.

Figure 8 shows the expected relative uncertainty for the VBS $Z_L Z_L$ fraction measurement as a function of the integrated luminosity and for the YR18 scenario described in Section 6 with a 10% uncertainty in the ggZZ loop-induced background yield. The effect of systematic uncertainties is negligible. The result is also shown for an integrated luminosity of 6000 fb$^{-1}$, which would approximately correspond to combining ATLAS and CMS after 3000 fb$^{-1}$.

Table 5 presents the expected significance and relative uncertainty in the VBS $Z_L Z_L$ fraction for various $\eta$ coverage configurations. The foreseen coverage extension of up to $|\eta| = 3(2.8)$ for electrons (muons) leads to a significant improvement for the significance and uncertainty in the VBS $Z_L Z_L$ fraction. An extension of up to $|\eta| = 4$ for electrons would allow to further improve by $\sim 4\%$ both the significance and the cross section measurement uncertainty.

Finally, a simple scaling of the signal and background cross sections is performed to assess the sensitivity to the VBS $Z_L Z_L$ fraction at HE-LHC. An integrated luminosity of 15 ab$^{-1}$ is

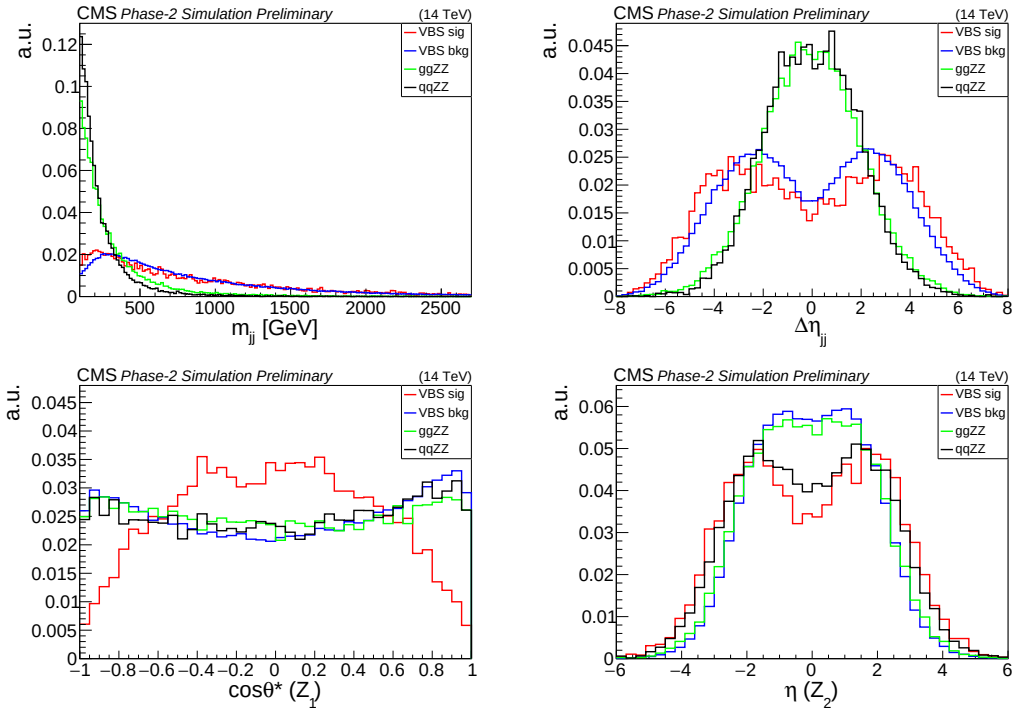


Figure 6: Distributions of some of the discriminant variables for the VBS $Z_LZ_L$ signal, the VBS $Z_LZ_T$ and $Z_TZ_T$ background and the QCD backgrounds from Delphes simulation and for the ZZjj inclusive selection that requires $m_{jj} > 100\,\text{GeV}$. The distributions are normalized to unity for shape comparison.

Table 5: Significance and measurement uncertainty in the VBS $Z_LZ_L$ fraction for different lepton coverage configurations. The first configuration corresponds to the Run 2 configuration, the second to the Phase-2 upgrade and the third to an option for which the electron coverage would be extended up to $|\eta| = 4$. In the quoted $\eta$ coverages, the first number corresponds to electrons, while the number in parentheses corresponds to muons.

| $\eta$ coverage | significance | VBS $Z_LZ_L$ fraction uncertainty (%) |
|---|---|---|
| $\|\eta\| < 2.5(2.4)$ | $1.22\sigma$ | 88 |
| $\|\eta\| < 3.0(2.8)$ | $1.38\sigma$ | 78 |
| $\|\eta\| < 4.0(2.8)$ | $1.43\sigma$ | 75 |

considered, together with a c.o.m energy of 27 TeV. The cross section ratios $\sigma_{27\,\text{TeV}}$ / $\sigma_{14\,\text{TeV}}$ are evaluated at LO with MADGRAPH (v5.4.2) [16] for the EW signal and the QCD qqZZ background, and with MCFM [28] for the QCD ggZZ background and reported in Table 1.

Table 6 shows the expected significance and relative uncertainty for the measurement of the VBS $Z_LZ_L$ fraction at HE-LHC, compared to HL-LHC. The HE-LHC machine would allow to bring the sensitivity (uncertainty) for the measurement of the VBS $Z_LZ_L$ fraction at the level of $\sim 5\sigma$ ($\sim 20\%$).

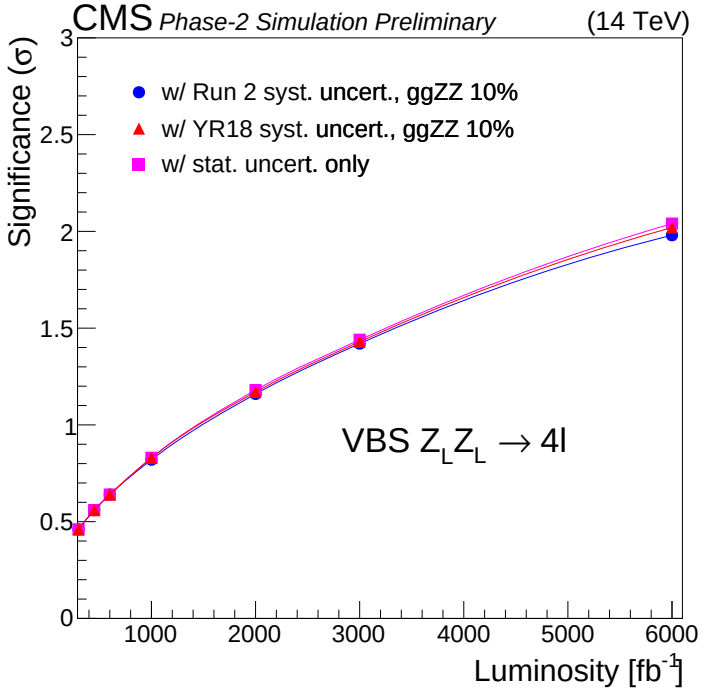


Figure 7: Expected significance for the VBS $Z_L Z_L$ fraction as a function of the integrated luminosity and for systematic uncertainties according to the Run 2 scenario (blue line and circles), and according to the YR18 scenario (red line and triangles). Results are shown for 10% uncertainty in the QCD ggZZ background yield. The magenta line and squares show the results with only the statistical uncertainties included.

Table 6: Expected significance and measurement uncertainty for the measurement of the VBS $Z_L Z_L$ fraction at HL-LHC and HE-LHC, with and without systematic uncertainties included.

| | significance | | VBS $Z_L Z_L$ fraction uncertainty (%) | |
|---|---|---|---|---|
| | w/ syst. uncert. | w/o syst. uncert. | w/ syst. uncert. | w/o syst. uncert.) |
| HL-LHC | $1.4\sigma$ | $1.4\sigma$ | 75% | 75% |
| HE-LHC | $5.2\sigma$ | $5.7\sigma$ | 20% | 19% |

# 10 Summary

We presented prospective studies for the vector boson scattering at the HL-LHC in the ZZ fully leptonic decay channel.

The analysis is based on the measurement performed using data recorded by the CMS experiment in 2016. The results previously obtained are projected to the expected integrated luminosity at HL-LHC of 3000 fb$^{-1}$ at the center-of-mass energy of 14 TeV, taking into account the increased acceptance of the new detector for the leptons and considering two scenario for the systematic uncertainties. The projected relative uncertainty in the VBS ZZ cross section measurement is 9.8% (8.8%) for the Run 2 (YR18) scenario and for a 10% uncertainty in the QCD ggZZ background yield, for an integrated luminosity of 3000 fb$^{-1}$ and a coverage of up to $|\eta| = 3$ for electrons. Extending the coverage up to $|\eta| = 4$ for electrons, the projected measurement uncertainty would be 9.5% and 8.5%, respectively.

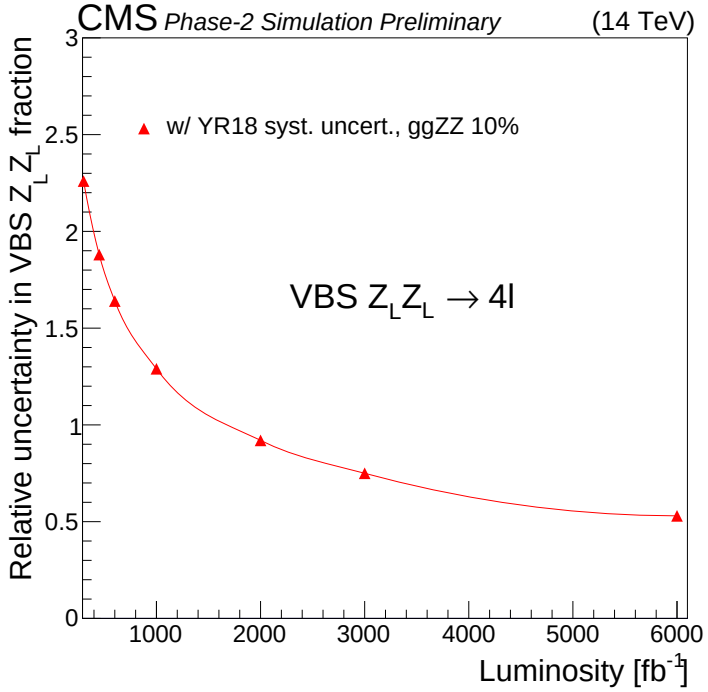


Figure 8: Expected relative uncertainty in the VBS $Z_L Z_L$ fraction as a function of the integrated luminosity and for systematic uncertainties according to the YR18 scenario. Results are shown for 10% uncertainty in the QCD ggZZ background yield.

The sensitivity for the longitudinal scattering VV $\rightarrow Z_L Z_L$ is assessed. The VBS $Z_L Z_L$ signal is separated from the VBS and QCD backgrounds by means of a multivariate discriminant that combines observables that discriminate VBS from QCD processes as well as observables that discriminate longitudinal from transverse Z boson polarizations. The expected significance for the VBS $Z_L Z_L$ fraction is $1.4\sigma$ for an integrated luminosity of 3000 fb$^{-1}$. With such integrated luminosity we enter measurement era for the VBS $Z_L Z_L$ fraction, with relative uncertainty below 100%. The measurement of such rare processes will of course benefit greatly of the highest luminosities. The lepton pseudorapidity coverage foreseen for the CMS detector upgrade leads to a significant improvement of the significance and cross section uncertainty for the VBS $Z_L Z_L$ process. Extending the coverage for electrons up to $|\eta| = 4$ would result in a modest improvement in the performance. Finally, the HE-LHC option would allow to bring the sensitivity at the $5\sigma$ level for this process.

## References

[1] CMS Collaboration, "Measurement of vector boson scattering and constraints on anomalous quartic couplings from events with four leptons and two jets in proton-proton collisions at sqrt(s) = 13 TeV.", *Phys. Lett. B* **774** (Aug, 2017) 682–705. 24 p, doi:10.1016/j.physletb.2017.10.020, arXiv:1708.02812.

[2] CMS Collaboration, "Observation of electroweak production of same-sign W boson pairs in the two jet and two same-sign lepton final state in proton-proton collisions at $\sqrt{s} = 13$ TeV", *Phys. Rev. Lett.* **120** (2018), no. 8, 081801, doi:10.1103/PhysRevLett.120.081801, arXiv:1709.05822.

[3] ATLAS Collaboration, "Observation of electroweak production of a same-sign $W$ boson pair in association with two jets in $pp$ collisions at $\sqrt{s} = 13$ TeV with the ATLAS detector", Technical Report ATLAS-CONF-2018-030, CERN, Geneva, Jul, 2018.

[4] ATLAS Collaboration, "Observation of electroweak $W^{\pm}Z$ boson pair production in association with two jets in pp collisions at $\sqrt{s}$ = 13TeV with the ATLAS Detector", Technical Report ATLAS-CONF-2018-033, CERN, Geneva, Jul, 2018.

[5] Ballestrero, A. and Maina, E. and Pelliccioli, G., "W polarization in vector boson scattering at the LHC", (2017). arXiv:1710.09339. Submitted to.

[6] DELPHES 3 Collaboration, "DELPHES 3, A modular framework for fast simulation of a generic collider experiment", *JHEP* **02** (2014) 057, doi:10.1007/JHEP02(2014)057, arXiv:1307.6346.

[7] G. Apollinari et al., "High-Luminosity Large Hadron Collider (HL-LHC) : Preliminary Design Report", doi:10.5170/CERN-2015-005.

[8] CMS Collaboration, "The CMS Experiment at the CERN LHC", *JINST* **3** (2008) S08004, doi:10.1088/1748-0221/3/08/S08004.

[9] CMS Collaboration, "Technical Proposal for the Phase-II Upgrade of the CMS Detector", Technical Report CERN-LHCC-2015-010. LHCC-P-008. CMS-TDR-15-02, 2015.

[10] CMS Collaboration, "The Phase-2 Upgrade of the CMS Tracker", Technical Report CERN-LHCC-2017-009. CMS-TDR-014, 2017.

[11] CMS Collaboration, "The Phase-2 Upgrade of the CMS Barrel Calorimeters Technical Design Report", Technical Report CERN-LHCC-2017-011. CMS-TDR-015, CERN, Geneva, Sep, 2017.

[12] CMS Collaboration, "The Phase-2 Upgrade of the CMS Endcap Calorimeter", Technical Report CERN-LHCC-2017-023. CMS-TDR-019, CERN, Geneva, Nov, 2017.

[13] CMS Collaboration, "The Phase-2 Upgrade of the CMS Muon Detectors", Technical Report CERN-LHCC-2017-012. CMS-TDR-016, CERN, Geneva, Sep, 2017.

[14] CMS Collaboration, "Particle-flow reconstruction and global event description with the CMS detector", (2017). arXiv:1706.04965. Submitted to JINST.

[15] CMS Collaboration, "CMS Phase-2 Object Performance", CMS Physics Analysis Summary, in preparation.

[16] J. Alwall et al., "MadGraph 5: going beyond", *JHEP* **06** (2011) 128, doi:10.1007/JHEP06(2011)128, arXiv:1106.0522.

[17] NNPDF Collaboration, "Parton distributions for the LHC Run II", *JHEP* **04** (2015) 040, doi:10.1007/JHEP04(2015)040, arXiv:1410.8849.

[18] J. Alwall et al., "The automated computation of tree-level and next-to-leading order differential cross sections, and their matching to parton shower simulations", *JHEP* **07** (2014) 079, doi:10.1007/JHEP07(2014)079, arXiv:1405.0301.

[19] R. Frederix and S. Frixione, "Merging meets matching in MC@NLO", *JHEP* **12** (2012) 061, doi:10.1007/JHEP12(2012)061, arXiv:1209.6215.

[20] T. Sjöstrand, S. Mrenna, and P. Skands, "Pythia 6.4 physics and manual", *JHEP* **05** (2006) 026, doi:10.1088/1126-6708/2006/05/026, arXiv:hep-ph/0603175.

[21] T. Sjöstrand et al., "An introduction to PYTHIA 8.2", *Comput. Phys. Commun.* **191** (2015) 159, doi:10.1016/j.cpc.2015.01.024, arXiv:1410.3012.

[22] CMS Collaboration, "Measurement of the ZZ production cross section and $Z \to \ell^+\ell^-\ell'^+\ell'^-$ branching fraction in pp collisions at $\sqrt{s} = 13\,\text{TeV}$", *Phys. Lett. B* **763** (2016) 280, doi:10.1016/j.physletb.2016.10.054, arXiv:1607.08834.

[23] D. Rainwater, R. Szalapski, and D. Zeppenfeld, "Probing color singlet exchange in $Z$+2-jet events at the CERN LHC", *Phys. Rev. D* **54** (1996) 6680, doi:10.1103/PhysRevD.54.6680, arXiv:hep-ph/9605444.

[24] CMS Collaboration, "Measurement of electroweak production of two jets in association with a Z boson in proton–proton collisions at $\sqrt{s} = 8\,\text{TeV}$", *Eur. Phys. J. C* **75** (2015) 66, doi:10.1140/epjc/s10052-014-3232-5, arXiv:1410.3153.

[25] Y. Gao et al., "Spin determination of single-produced resonances at hadron colliders", *Phys. Rev. D* **81** (2010) 075022, doi:10.1103/PhysRevD.81.075022, arXiv:1001.3396. [Erratum: *Phys. Rev. D* **81** (2010) 079905 doi:10.1103/PhysRevD.81.079905].

[26] S. Bolognesi et al., "Spin and parity of a single-produced resonance at the LHC", *Phys. Rev. D* **86** (2012) 095031, doi:10.1103/PhysRevD.86.095031, arXiv:1208.4018.

[27] I. Anderson et al., "Constraining anomalous $HVV$ interactions at proton and lepton colliders", *Phys. Rev. D* **89** (2014) 035007, doi:10.1103/PhysRevD.89.035007, arXiv:1309.4819.

[28] J. M. Campbell and R. K. Ellis, "MCFM for the Tevatron and the LHC", *Nucl. Phys. B Proc. Suppl.* **205-206** (2010) 10, doi:10.1016/j.nuclphysbps.2010.08.011, arXiv:1007.3492.

[29] F. Campanario, M. Kerner, L. D. Ninh, and D. Zeppenfeld, "Next-to-leading order QCD corrections to ZZ production in association with two jets", *JHEP* **07** (2014) 148, doi:10.1007/JHEP07(2014)148, arXiv:1405.3972.

[30] M. Botje et al., "The PDF4LHC Working Group Interim Recommendations", arXiv:1101.0538.

[31] S. Alekhin et al., "The PDF4LHC Working Group Interim Report", arXiv:1101.0536.

[32] NNPDF Collaboration, "Parton distributions for the LHC run II", *JHEP* **04** (2015) 040, doi:10.1007/JHEP04(2015)040, arXiv:1410.8849.